# PoseGen: In-Context LoRA Finetuning for Pose-Controllable Long Human Video Generation

# Jingxuan He<sup>1</sup>, Busheng Su<sup>1</sup>, Finn Wong<sup>1\*</sup>

<sup>1</sup>Xiaoice

{hejingxuan, subusheng, wangwenlan}@xiaobing.ai {jingxuanhe1210, bushengsu, fantasyfw}@gmail.com

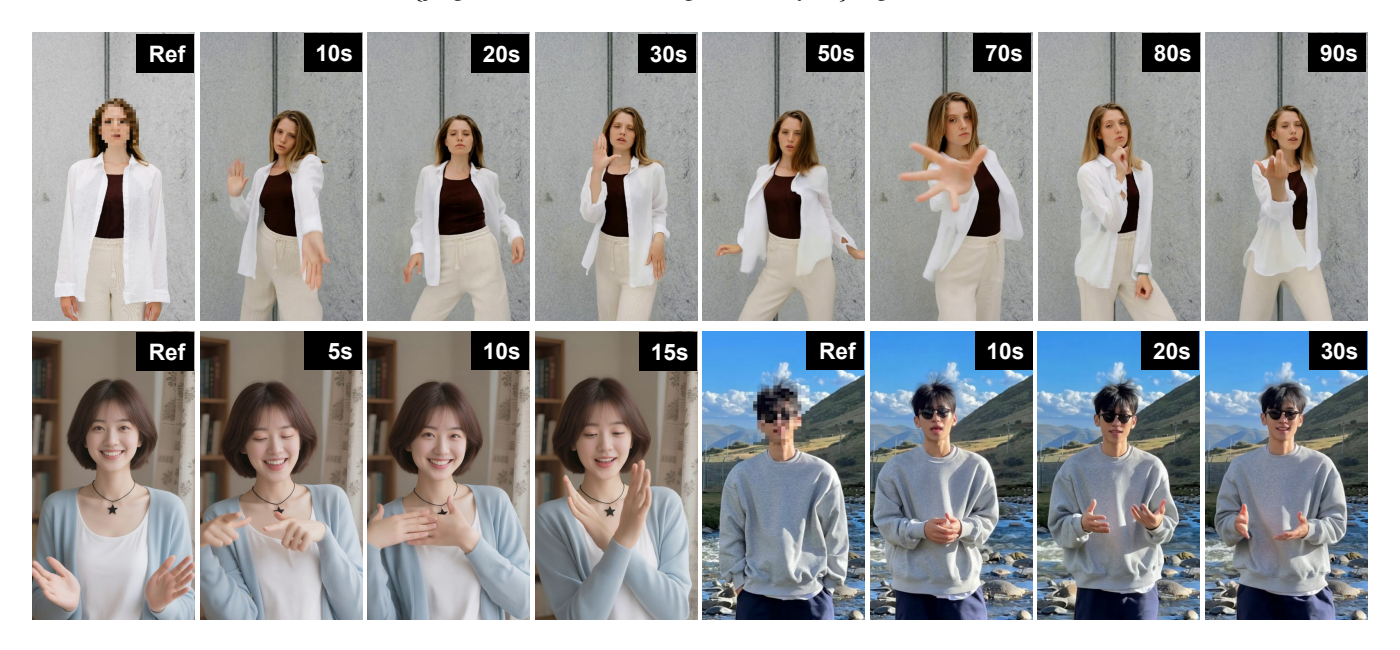


Figure 1: We present PoseGen, a pose-controllable human video generation framework that is capable of generating arbitrarily long videos from a human reference image and a driving pose sequence. Our framework maintains visual fidelity to the reference appearance while ensuring temporal coherence throughout the whole synthesized video.

#### **Abstract**

Generating long, temporally coherent videos with precise control over subject identity and motion is a formidable challenge for current diffusion models, which often suffer from identity drift and are limited to short clips. We introduce PoseGen, a novel framework that generates arbitrarily long videos of a specific subject from a single reference image and a driving pose sequence. Our core innovation is an incontext LoRA finetuning strategy that injects subject appearance at the token level for identity preservation, while simultaneously conditioning on pose information at the channel level for fine-grained motion control. To overcome duration limits, PoseGen pioneers an interleaved segment generation method that seamlessly stitches video clips together, using a shared KV cache mechanism and a specialized transition process to ensure background consistency and temporal smoothness. Trained on a remarkably small 33-hour video dataset, extensive experiments show that PoseGen significantly outperforms state-of-the-art methods in identity fidelity, pose accuracy, and its unique ability to produce coherent, artifactfree videos of unlimited duration.

#### 1 Introduction

The synthesis of high-fidelity video content has emerged as a key frontier in generative AI, propelled by the remarkable success of diffusion models in image generation (Rombach et al. 2022). The ability to automatically create realistic and controllable videos holds transformative potential for industries ranging from entertainment and filmmaking to virtual reality and marketing. Although text-to-video (T2V) models (Kong et al. 2024; Wan et al. 2025) have demonstrated impressive quality, they often lack the fine-grained controllability necessary for many practical applications. A critical need exists for methods capable of generating videos from text prompts while preserving subject identity and enabling precise, long-duration motion control.

This need has spurred research into controllable video generation (Hu et al. 2025; Jiang et al. 2025). However, significant challenges in controllability and duration persist. Existing methods struggle with three core issues: 1) Identity Drift: The subject's appearance often morphs over time. 2) Motion Inaccuracy: Precise control over subject motion,

<sup>\*</sup>Corresponding Author

such as following a specific pose sequence without artifacts, remains difficult. 3) Limited Duration: Most models are architecturally confined to short clips (typically less than 10s), with longer generation attempts leading to severe degradation in temporal coherence and the accumulation of structural errors, especially in fine-grained regions such as hands. Furthermore, a significant, yet often overlooked, challenge is the immense computational cost and data appetite of current state-of-the-art models. Many leading frameworks require massive, proprietary datasets up to 10K+ hours for training. This not only makes them extremely resource intensive and expensive to reproduce, but also limits their accessibility to researchers and smaller teams, posing a major barrier to innovation and practical application.

To overcome these significant hurdles, we propose PoseGen, a new paradigm for pose-controllable long video generation from a single reference image. PoseGen leverages the efficiency of LoRA (Hu et al. 2022) to finetune a pretrained video diffusion model (Wan et al. 2025). Our key insight is a dual conditioning mechanism we term "incontext LoRA finetuning". To preserve subject identity, we encode the reference image into VAE latents and concatenate them with the noise latents along the token dimension, directly providing appearance context. For motion control, we concatenate the latents of the target pose skeletons and hand normal maps with the noise latents along the channel dimension, guiding the generation frame-by-frame.

PoseGen's primary contribution is its ability to generate videos of arbitrary length without identity drift or temporal inconsistency. We achieve this through a novel segment-based strategy. The video is first generated as multiple independent, interleaved short segments. Background consistency is maintained by caching and reusing the Key-Value (KV) pairs from the self-attention layers of a source segment (Cao et al. 2023; Cai et al. 2025). Seamless transitions are then created by dedicated "stitching" segments that interpolate between the primary segments.

To support this modular architecture, we adopt two separate LoRA modules trained for distinct purposes. The first is trained to generate the main content segments from the reference image and pose sequence. The second is trained specifically for the interpolation task, creating smooth stitching segments to connect the main parts. This dual-task approach ensures the generation of coherent and long-form videos. Our main contributions can be summarized as follows:

- We propose PoseGen, a novel and efficient framework for generating high-fidelity, pose-controllable videos of unlimited length from a single reference image.
- We introduce a dual in-context conditioning mechanism that injects appearance identity at the token level and pose guidance at the channel level, achieving superior subject fidelity and motion control.
- We pioneer an interleaved segment generation and stitching method that leverages KV cache sharing for background consistency, effectively addressing the long video generation problem.
- We demonstrate through comprehensive quantitative and qualitative comparisons that PoseGen surpasses state-of-

the-art controllable video generation models, including MimicMotion (Zhang et al. 2025), StableAnimator (Tu et al. 2025), DisPose (Li et al. 2024), HumanDiT (Gan et al. 2025), and UniAnimate-DiT (Wang et al. 2025) in quality, control, temporal coherence and video duration.

#### 2 Related Work

### 2.1 Identity-Consistent Video Generation

A primary challenge in video synthesis is maintaining the identity of a subject provided in a reference image. Early approaches adapted techniques from image personalization, such as DreamBooth (Ruiz et al. 2023), which finetunes the entire model for a specific subject, leading to high storage costs and slow adaptation. More efficient methods leverage parameter-efficient finetuning. For instance, DreamActor-M1 (Luo et al. 2025) and VACE (Jiang et al. 2025) utilize tailored network adaptations and attention mechanisms to inject identity features into a base T2V model. OmniHuman-1 (Lin et al. 2025) and HunyuanVideo-Avatar (Chen et al. 2025) build audio driven human-centric generation systems through hybrid training strategies and multiple injection modules with face masking, respectively. However, these methods often require multiple reference images, complex preprocessing pipelines, or intricate architectural designs and training schemes. PoseGen distinguishes itself by using a simple yet powerful in-context LoRA training approach, which is not only efficient but also highly effective at preventing identity drift, even in very long videos.

#### 2.2 Pose and Motion Controllable Generation

Controlling the motion of a generated subject is crucial for creating dynamic and purposeful content. A significant line of work conditions video diffusion models on explicit control signals like skeletal poses (Cao et al. 2019), depth maps, or edge maps, inspired by the success of ControlNet (Zhang, Rao, and Agrawala 2023) in image synthesis. AnimateDiff (Guo et al. 2024) introduced a motion module that could be plugged into existing text-to-image models to generate temporal animations. Building on this, Animate Anyone (Hu 2024) and UniAnimate (Wang et al. 2024) proposed more sophisticated architectures specifically designed for human animation, often using separate encoders for appearance and pose. Recent works have explored leveraging the scalability of DiT (Peebles and Xie 2022) architectures for better performance. Nevertheless, the computational demands of modeling long temporal sequences present a significant bottleneck. PoseGen addresses this limitation through a lightweight yet effective channel-wise pose conditioning mechanism that integrates seamlessly into our architecture. Motion control is achieved using two complementary pathways: the first generates identity-consistent segments from a reference image and according pose sequence, while the second specializes in synthesizing smooth transitions between segments using first/last frame constraints and intermediate poses. This dual-pathway design enables robust, long-range motion control without requiring heavyweight architecture changes or sacrificing subject consistency over time.

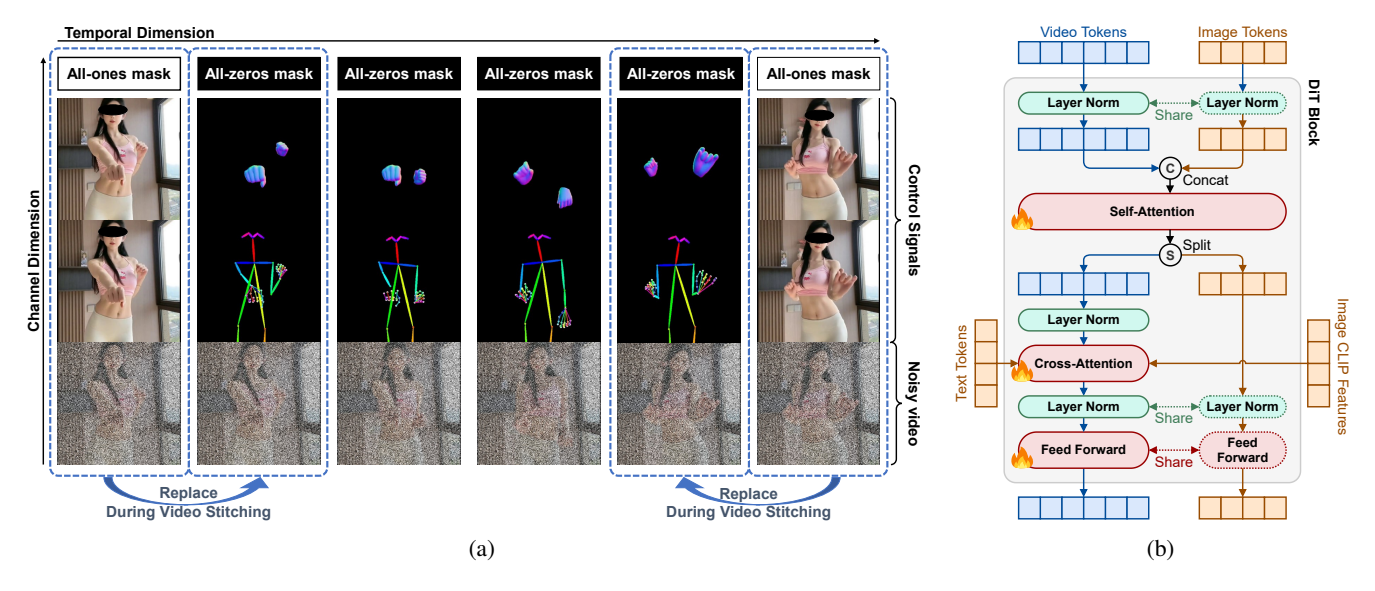


Figure 2: Overview of in-context LoRA finetuning. (a) Motion control. We adopt pose skeletons and hand surface normals as control signals. These conditions are concatenated with noisy video frames in the latent space. (b) Reference injection. Image and video tokens are processed through a stack of DiT blocks with shared parameters. LoRA is applied to the self-attention, cross-attention, and feed forward layers in each DiT block.

## 2.3 Long Video Generation

Extending video generation beyond a few seconds is a notoriously difficult problem due to the compounding errors and memory constraints in autoregressive or single-pass generation for DiT models. Some methods attempt to generate longer videos in a single shot but are often restricted to simpler content, such as portrait videos where the background is static or blurry, thus simplifying the coherence challenge. Other approaches involve hierarchical generation or video interpolation, which can create visible artifacts or lack fine-grained control (Zhang et al. 2025; Qiu et al. 2023; Henschel et al. 2025). Our interleaved segment generation method presents a new path forward. While sharing the KV cache to maintain consistency has been explored for internal frame attention in DiTCtrl (Cai et al. 2025), we are the first to adapt this concept to enforce background consistency across independently generated video segments. This, combined with our specialized frame-stitching process, allows PoseGen to be the first framework, to our knowledge, capable of producing coherent, controllable, and unlimited long videos in a general-purpose setting.

## 3 Method

Given a reference image and a driving video, PoseGen synthesizes a video of the subject following the specified motion, preserving human and background consistency.

#### 3.1 Preliminaries

Our method is built on Diffusion Transformers (DiTs) (Peebles and Xie 2023), which combine strong generation capabilities of diffusion models (Sohl-Dickstein et al. 2015; Ho, Jain, and Abbeel 2020) with the expressiveness and scalability of Transformers (Vaswani et al. 2017). Modern diffusion models designed for video synthesis (Yang et al. 2024b; Wan

et al. 2025) typically employ a causal 3D Variational Auto-Encoder (VAE) to compress videos from pixel space to latent space, in order to reduce computational complexity and memory consumption. The 3D VAE is composed of an encoder  $\mathcal{E}$  and a decoder  $\mathcal{D}$ , where the encoder compresses a video  $\mathbf{x} \in \mathbb{R}^{3\times F\times H\times W}$  into its corresponding video latents  $\mathbf{z} = \mathcal{E}(\mathbf{x}) \in \mathbb{R}^{c\times f\times h\times w}$  and the decoder projects the video latents back to the original pixels  $\mathbf{x} = \mathcal{D}(\mathbf{z}) \in \mathbb{R}^{3\times F\times H\times W}$ . Here F, H, and W denote the number of frames, height, and width, respectively. For Wan2.1 (Wan et al. 2025), the latents have c=16 channels, with a temporal length of f=(F-1)/4+1, latent height h=H/8, and latent width w=W/8.

A DiT denoising model consists of three major modules: a patchifier, a stack of Transformer blocks, and an unpatchifier. The patchifier applies 3D convolutions with a kernel size of (1,2,2) to embed video latents  $\mathbf{z}$  into a sequence of video tokens  $\mathbf{t} \in \mathbb{R}^{n \times d}$ , where d is the token embedding dimension, and  $n = (f/1) \cdot (h/2) \cdot (w/2)$ . Additionally, text prompts are embedded through cross-attention following the self-attention operation in each Transformer block.

#### 3.2 In-Context LoRA Finetuning

Our in-context LoRA finetuning is a dual conditioning mechanism that simultaneously facilitates pose-guided human animation and visual appearance preservation. It is a simple yet effective solution with minimal architectural modifications to the underlying diffusion model.

**Motion Control.** To achieve pose-guided motion control, we adopt pose skeleton images as the primary driving signals following established practices in prior works (Hu 2024; Zhang et al. 2025; Tu et al. 2025). However, in our early experiments, we observed that the synthesized videos often suffered from degraded quality in hand regions due

to their high-frequency textures and rapid movements. To mitigate this issue, as presented in Fig. 2 (a), we introduce hand surface normals as auxiliary control signals. These normals are estimated using a surface normal prediction model in combination with a body-part segmentation model (Khirodkar et al. 2024). This approach is advantageous as surface normals offer rich geometric cues to handle difficult cases like overlapping hands, where mesh-based estimation often struggles (Zhou et al. 2024). To condition the diffusion model on these control signals, we concatenate pose skeleton and hand normal images with the noisy video along the channel dimension in latent space. Additionally, to enable pose-aware frame interpolation for long video generation, we introduce a masking mechanism to specify which frames are to be synthesized. Specifically, we adopt a binary mask  $\mathbf{m} \in \{0,1\}^{s \times f \times h \times w}$  in which a value of 0 indicates frames to be generated and a value of 1 signifies frames to be preserved. Here s is the temporal stride of the causal 3D VAE. For the base phase of pose-guided video generation, the mask m is filled with zeros, while for the interpolation phase that stitches video segments together, the positions of the first few and last few frames are marked with ones. Given the noisy video latents  $\mathbf{z}_{\text{vid}} \in \mathbb{R}^{c \times f \times h \times w}$ , pose skeleton latents  $\mathbf{z}_{\text{pose}} \in \mathbb{R}^{c \times f \times h \times w}$ , and hand normal latents  $\mathbf{z}_{\text{hand}} \in \mathbb{R}^{c \times f \times h \times w}$ , the video tokens  $\mathbf{t}_{\text{vid}} \in \mathbb{R}^{n_{\text{vid}} \times d}$  with sequence length  $n_{\rm vid} = (f/1) \cdot (h/2) \cdot (w/2)$  are obtained as follows:

$$\mathbf{t}_{\text{vid}} = \text{Patchifier}([\mathbf{z}_{\text{vid}}; \mathbf{m}; \mathbf{z}_{\text{pose}}; \mathbf{z}_{\text{hand}}]),$$
 (1)

where [;] denotes concatenation along the channel axis, and Patchifier() is a patch embedding layer instantiated with 3D convolutions.

**Reference Injection.** To ensure that the synthesized video remains consistent with the subject's appearance depicted in the reference image, we propose an architecture-efficient method to inject the reference information into the modeling process. We first compress the reference image into its image latents  $\mathbf{z}_{\text{img}} \in \mathbb{R}^{c \times 1 \times h \times w}$  using the same pretrained VAE. A separate patchifier is applied to convert the image latents  $\mathbf{z}_{\text{img}}$  into image tokens  $\mathbf{t}_{\text{img}} \in \mathbb{R}^{n_{\text{img}} \times d}$  with sequence length  $n_{\text{img}} = (h/2) \cdot (w/2)$ . As shown in Fig. 2 (b), image tokens  $\mathbf{t}_{img}$  and video tokens  $\mathbf{t}_{vid}$  are processed in parallel through a stack of DiT blocks. In each DiT block, two sets of tokens pass through self-attention and feed forward layers that share the same parameters. During self-attention, we concatenate video and image tokens along the sequence dimension and perform full self-attention. Specifically, video and image tokens are linearly projected to queries Q, keys K, and values V. Rotary Position Embedding (RoPE) (Su et al. 2024) is subsequently applied to gueries and keys to provide positional information. Inspired by OminiControl (Tan et al. 2024), we shift the position indices of image tokens to avoid overlap with those of the video tokens, considering that the reference image and the synthesized frames are not strictly spatially aligned. The full self-attention of layer l is then computed as:

$$Attn([\mathbf{t}_{vid}^{(l)}; \mathbf{t}_{img}^{(l)}]) = Softmax\left(\frac{\mathbf{Q}^{(l)}\mathbf{K}^{(l)^{\top}}}{\sqrt{d}}\right)\mathbf{V}^{(l)}. \quad (2)$$

Algorithm 1: Inference-Time Background KV-Sharing

**Input**: Initial video tokens  $\mathbf{t}_{\mathrm{vid}}$ ; cached source keys  $\{\mathbf{K}_{\mathrm{src}}^{(l,t)}\}$ and source values  $\{\mathbf{V}_{\rm src}^{(l,t)}\}$ 1: **for** t = T, T - 1, ..., 1 **do** for  $l=1,2\ldots,L$  do  $\hat{\mathbf{t}}_{\mathrm{vid}}^{(l,t)} \leftarrow \mathrm{Attn}([\mathbf{t}_{\mathrm{vid}}^{(l,t)}; \mathbf{t}_{\mathrm{img}}^{(l,t)}])$  **if** Background KV-Sharing **then** ⊳ Eq. (2) 3: 4:  $\begin{aligned} \mathbf{M}^{(l,t)} &\leftarrow \mathbf{Q}_{\text{text}}^{(l,t)}, \mathbf{K}_{\text{vid}}^{(l,t)} \\ \mathbf{M}_{\text{src}}^{(l,t)} &\leftarrow \mathbf{Q}_{\text{text,src}}^{(l,t)}, \mathbf{K}_{\text{vid,src}}^{(l,t)} \\ \hat{\mathbf{t}}_{\text{vid,src}}^{(l,t)} &\leftarrow \mathbf{Q}_{\text{text,src}}^{(l,t)}, \mathbf{K}_{\text{vid,src}}^{(l,t)} \\ \hat{\mathbf{t}}_{\text{vid,src}}^{(l,t)} &\leftarrow \operatorname{Attn}([\mathbf{t}_{\text{vid}}^{(l,t)}; \mathbf{t}_{\text{img}}^{(l,t)}]; \mathbf{M}_{\text{src}}^{(l,t)}) \end{aligned}$ 5: ⊳ Eq. (4) 6: ⊳ Eq. (4) 7: ⊳ Eq. (5) Update  $\hat{\mathbf{t}}_{\mathrm{vid}}^{(l,t)}$ 8: ⊳ Eq. (6) 9:  $\mathbf{t}_{\mathrm{vid}}^{(l+1,t)} \leftarrow \mathrm{FeedForward}\left(\hat{\mathbf{t}}_{\mathrm{vid}}^{(l,t)}\right)$ 10:  $\begin{array}{ll} \textbf{11:} & \textbf{end for} \\ \textbf{12:} & \textbf{t}_{\text{vid}}^{(1,t-1)} \leftarrow \textbf{t}_{\text{vid}}^{(L,t)} \\ \textbf{13:} & \textbf{end for} \end{array}$ 

**Return**: Denoised video tokens  $\mathbf{t}_{vid}$ 

To enhance semantic understanding of the visual content, the video tokens additionally interact with text embeddings and CLIP (Radford et al. 2021) features of the reference image after full self-attention.

LoRA Finetuning. Our approaches to motion control and reference injection inherently support parameter-efficient LoRA (Hu et al. 2022) finetuning. First, the channel-wise concatenation used in motion control imposes spatial alignment between guidance and generation, which effectively reduces the complexity of the learning process. Second, the sequence-wise concatenation adopted in reference injection enables flexible token-level interactions, leveraging the strong contextual modeling capabilities of the DiT architecture. During finetuning, we optimize LoRA parameters applied to the self-attention, cross-attention, and feed forward layers in DiT blocks, as well as the newly introduced parameters in patchifiers.

## 3.3 Long Video Generation

A significant challenge in generating long videos is maintaining continuity across different segments. Naively generating a long video by sequentially composing short clips fails for two primary reasons. First, pose skeletons alone lack the appearance details to ensure smooth transitions, leading to motion artifacts. Second, independently generated segments suffer from background drift as the subject moves, destroying the illusion of a continuous scene.

To address these issues, we propose a novel interleaved video segment generation strategy coupled with background KV-sharing. Our process begins by first generating disjoint video segments at regular intervals. Then, we generate the "in-between" segments using a specialized LoRA model trained for interpolation, effectively stitching the key segments together into a single, seamless video.

The core idea for maintaining background consistency is to cache and reuse background key-value pairs from the self-

Method	L1 (E-5) ↓	PSNR ↑	SSIM ↑	LPIPS ↓	FID ↓	FID-VID↓	FVD↓
MimicMotion ICML 2025	3.20/3.33	17.79/17.85	0.775/0.760	0.251/0.292	47.36/63.05	20.58/20.00	348.26/381.67
DisPose ICLR 2025	3.09/3.31	18.04/18.07	0.794/0.783	0.247/0.276	50.91/67.88	16.83/24.08	387.37/409.85
StableAnimator CVPR 2025	3.42/4.06	17.26/16.55	0.755/0.719	0.264/0.310	51.74/67.33	18.89/22.98	460.35/436.79
UniAnimate-DiT arXiv 2025	2.03/2.15	20.59/17.54	<b>0.828</b> /0.794	0.194/0.286	43.19/ <b>52.36</b>	29.40/19.98	280.59/282.43
HumanDiT <sub>arXiv 2025</sub>	2.17/ <b>1.61</b>	<b>21.79</b> /19.78	0.824/ <b>0.821</b>	0.152/0.241	38.97/62.48	10.62/15.77	216.20/349.05
PoseGen (Ours)	1.96/1.61	20.91/ <b>20.24</b>	0.814/ <b>0.821</b>	0.172/0.242	<b>38.67</b> /53.63	10.25/14.21	210.75/214.51

Table 1: Quantitative comparison with state-of-the-art methods. Results are presented as scores on the TikTok/PoseGen-Val (Same-ID) datasets. For all metrics, ↑ indicates higher is better, and ↓ indicates lower is better.

Method	Visual Quality ↑	Identity Preservation ↑	Temporal Consistency	
MimicMotion	78.49	84.02	93.33	
DisPose	79.48	87.01	93.71	
StableAnimator	86.38	84.81	92.33	
UniAnimate-DiT	87.22	94.75	94.85	
HumanDiT	86.31	84.70	94.85	
PoseGen (Ours)	87.47	94.99	95.22	

Table 2: Quantitative results on PoseGen-Val (Cross-ID).

Method	Visual Quality ↑	Identity Preservation ↑	Temporal Consistency ↑
MimicMotion	2.52	2.43	2.76
DisPose	2.71	2.49	2.89
StableAnimator	2.87	2.54	2.73
UniAnimate-DiT	3.55	3.36	3.08
HumanDiT	3.45	2.79	3.53
PoseGen (Ours)	4.16	4.07	4.16

Table 3: User study results on PoseGen-Val (Cross-ID).

attention layers of a source segment (i.e., the first generated segment). To identify background regions, we derive binary masks from attention maps computed using queries and keys in cross-attention layers. Mathematically, given text queries  $\mathbf{Q}_{\text{text}}^{(l)} \in \mathbb{R}^{n_{\text{text}} \times d}$ , video keys  $\mathbf{K}_{\text{vid}}^{(l)} \in \mathbb{R}^{n_{\text{vid}} \times d}$ , and subject-relevant (e.g., "woman", "man") text token indices  $\mathbb{I} \subset \{0,\dots,n_{\text{text}}-1\}$ , the attention map  $\mathbf{A}^{(l)}$  and the corresponding attention mask  $\mathbf{M}^{(l)}$  are computed as:

$$\mathbf{A}^{(l)} = \frac{1}{|\mathbb{I}|} \sum_{i \in \mathbb{I}} \left( \frac{\mathbf{Q}_{\text{text},i}^{(l)} \mathbf{K}_{\text{vid}}^{(l)^{\top}}}{\sqrt{d}} \right), \tag{3}$$

$$\mathbf{M}^{(l)} = \frac{1}{l} \sum_{i=1}^{l} \text{Thresholding} \left( \mathbf{A}^{(i)} \right). \tag{4}$$

The resulting mask  $\mathbf{M}^{(l)}$  takes the value of 1 for subject regions and 0 for the background via Otsu's thresholding. Inspired by mutual self-attention (Cao et al. 2023), we reformulate the existing self-attention in Eq. (2) to facilitate information exchange between current and source segments. Specifically, in the l-th self-attention layer, the queries  $\mathbf{Q}^{(l)}$  remain unchanged, while the keys and the values are substituted with those from the corresponding self-attention layer

of the source segment (denoted as  $\mathbf{K}_{\mathrm{src}}^{(l)}$  and  $\mathbf{V}_{\mathrm{src}}^{(l)}$ ):

$$\operatorname{Attn}([\mathbf{t}_{\text{vid}}^{(l)}; \mathbf{t}_{\text{img}}^{(l)}]; \mathbf{M}_{\text{src}}^{(l)}) = \left[ \left( 1 - \mathbf{M}_{\text{src}}^{(l)} \right) \odot \operatorname{Softmax} \left( \frac{\mathbf{Q}^{(l)} \mathbf{K}_{\text{src}}^{(l)}^{\top}}{\sqrt{d}} \right) \right] \mathbf{V}_{\text{src}}^{(l)},$$
(5)

where  $\mathbf{M}_{\mathrm{src}}^{(l)}$  denotes the attention mask from the source segment computed analogously to  $\mathbf{M}^{(l)}$  in Eq. (4).  $\mathbf{M}_{\mathrm{src}}^{(l)}$  is introduced to exclusively extract background visual content. Subsequently, let  $\hat{\mathbf{t}}_{\mathrm{vid}}^{(l)}$  represent the updated video token embeddings after the self-attention layer, the embeddings are fused as follows:

$$\hat{\mathbf{t}}_{\text{vid}}^{(l)} \leftarrow \hat{\mathbf{t}}_{\text{vid}}^{(l)} \odot \left( \mathbf{M}^{(l)} \vee \mathbf{M}_{\text{src}}^{(l)} \right) + \\
\hat{\mathbf{t}}_{\text{vid,src}}^{(l)} \odot \left( 1 - \mathbf{M}^{(l)} \vee \mathbf{M}_{\text{src}}^{(l)} \right),$$
(6)

where  $\odot$  is the element-wise product,  $\vee$  is the OR operation to identify the common background in two segments. The background KV-sharing method is summarized in Alg. 1.

## 4 Experiments

## 4.1 Experimental Settings

Implementation Details. We use Sapiens (Khirodkar et al. 2024) for pose/hand normal extraction and build upon Wan2.1-I2V-14B (Wan et al. 2025). We finetune linear layers within self-attention, cross-attention, and feed forward modules in Wan2.1 using LoRA (rank=16) (Hu et al. 2022) on a self-collected 33-hour video dataset (7,005 videos), which is orders of magnitude smaller than prior works (Luo et al. 2025; Gan et al. 2025). The base LoRA was trained for 4,000 steps on 8 NVIDIA A100-SXM4-80GB GPUs with a batch size of 8, 720p resolution. The video stitching LoRA was trained to retain the first and last 1/4 frames while keeping other settings unchanged. Background KV-sharing is performed at initial denoising steps and deep layers following the configuration in DiTCtrl (Cai et al. 2025).

**Evaluation Metrics.** We use standard image-level (L1, PSNR, SSIM, LPIPS, FID) and video-level (FID-VID, FVD) metrics (Hore and Ziou 2010; Wang et al. 2004; Zhang et al. 2018; Heusel et al. 2017; Balaji et al. 2019; Unterthiner et al. 2018). For perceptual studies without ground truths, we measure visual quality with Q-Align (Wu et al. 2023), identity preservation with ArcFace (Deng et al. 2019), and temporal consistency with DINO feature similarity (Caron et al. 2021).



Figure 3: Qualitative comparison with state-of-the-art methods. The examples are from PoseGen-Val (Cross-ID). Our method demonstrates superior performance in preserving the subject's identity and detailed appearance.

## 4.2 Comparison with State-of-the-Art Methods

We compared PoseGen with state-of-the-art pose-driven human video generation methods that encompass both UNetbased and DiT-based architectures, including MimicMotion (Zhang et al. 2025), DisPose (Li et al. 2024), StableAnimator (Tu et al. 2025), UniAnimate-DiT (Wang et al. 2025), and HumanDiT (Gan et al. 2025). We conducted experiments on TikTok dataset (Jafarian and Park 2021) following prior works (Zhang et al. 2025; Li et al. 2024; Tu et al. 2025). To assess our model's performance beyond short TikTok clips, we created two custom validation sets for distinct purposes. For evaluating long-term temporal coherence, we introduced PoseGen-Val (Same-ID), which features 9 lengthy human movement videos. To test generalization against new identities, we built PoseGen-Val (Cross-ID). This more challenging set contains 13 pairs, each matching a video with a cross-identity reference image sourced from a mix of both real and AI-generated photos.

Quantitative Results. Tab. 1 shows the quantitative results on the TikTok and PoseGen-Val (Same-ID) datasets. As can be seen, PoseGen demonstrates superior performance over state-of-the-art methods across most metrics. It not only achieves the lowest L1 error, indicating higher pixel-wise accuracy, but also significantly outperforms on video-level metrics by notable margins (FID-VID and FVD). This highlights its strong capability for maintaining temporal consistency in perceptually realistic videos. The results on our more challenging PoseGen-Val (Cross-ID) set (Tab. 2) further underscore PoseGen's strengths. In these cross-identity cases, our method consistently surpasses all competitors across the three evaluated perceptual dimensions. For instance, while UniAnimate-DiT is competitive in visual quality and identity preservation, PoseGen's distinct advantage in temporal consistency directly validates the effectiveness of our proposed long-video generation strategy.

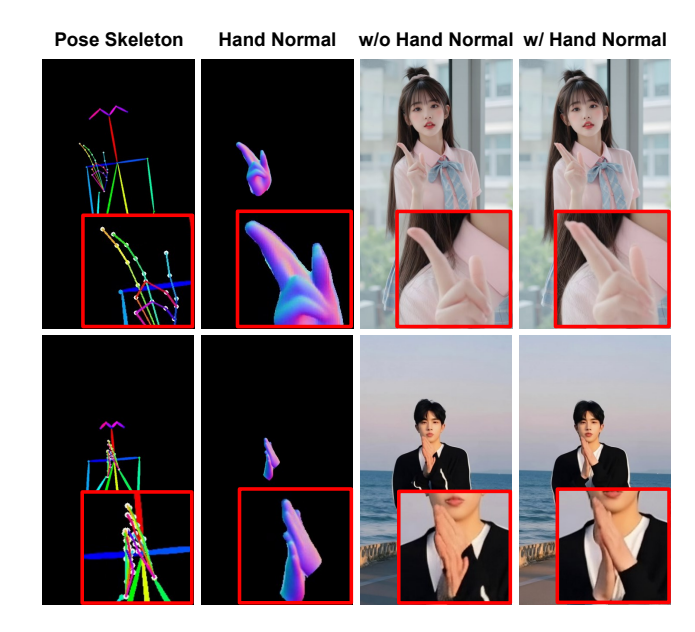


Figure 4: Ablation study of hand surface normals. Red boxes enlarge the hand region of interested.

Qualitative Results. As shown in Fig. 3, PoseGen excels at preserving a subject's identity and appearance details where other state-of-the-art methods falter. For instance, competing methods often fail to replicate clothing texture and color (top row) or distort complex traditional attire and facial features (bottom row). In contrast, PoseGen faithfully preserves these intricate details while ensuring coherent motion, yielding visually superior and more faithful results.

**User Study.** To evaluate perceptual quality, we conducted a user study comparing PoseGen against five other leading competitors on PoseGen-Val (Cross-ID). For this study, we



Figure 5: Ablation of background KV-sharing (BG KV) and attention masking. Background mismatches are highlighted.

invited 27 participants to rate 13 generated cross-identity videos on a scale of 0-5 in terms of three criteria: visual quality, identity preservation, and temporal consistency. Results summarized in Tab. 3 reveal a clear preference for PoseGen. Our method achieves the highest scores across all categories by a large margin, substantially outperforming others and demonstrating its superior ability to generate high-quality, coherent, and perceptually appealing videos.

#### 4.3 Ablation Study

Hand Surface Normals. To evaluate the effectiveness of hand surface normals as an additional driving signal beyond pose skeletons, we train a model variant that only conditions on pose skeletons. The comparison results are illustrated in Fig. 4. The example in the first row shows that dense surface normals complement sparse pose skeletons by providing nuanced shape information, which effectively prevents the unintended merging of distinct fingers. The example in the second row demonstrates that surface normals help disambiguate interactions between hands by capturing finegrained geometric details, resulting in anatomically plausible hand positions.

Background KV-Sharing. Background KV-sharing is a pivotal component of our method that facilitates smooth transitions across video segments for coherent long video generation. We ablate this component and its attention-based masking mechanism in Fig. 5. As can be seen, removing background KV-sharing results in slight but perceptible background shifts as the woman dances or the man mimics walking. While such variations are acceptable within a short video segment, they pose abnormal motions when we stitch multiple segments into a long video. Moreover, when the subject-background mask derived from cross-attention is removed, the background remains consistent with the target



Figure 6: Ablation study of long video generation. Each row displays frames of a video with over 10 seconds at 30 FPS. The reference image is presented at the bottom-left corner.

scene; however, the subject exhibits noticeable artifacts as a single frame blends two incompatible poses of the same person. These results underscore the effectiveness of our proposed background KV-sharing in preserving background consistency while faithfully guiding the subject's movement according to the provided pose.

Long Video Generation. We compare our interleaved generation and stitching framework against using the base model with training-free alternatives like FreeNoise (Qiu et al. 2023) and StreamingT2V (Henschel et al. 2025). As shown in Fig. 6, both alternatives fail to maintain background consistency. FreeNoise produces unstable backgrounds, while the autoregressive StreamingT2V suffers from error accumulation, causing background drift. In contrast, our method maintains high background fidelity across the entire sequence, demonstrating the effectiveness of our background KV-sharing and pose-aware interpolation.

## 5 Conclusion

In this work, we presented PoseGen, a computationally efficient framework for generating high-fidelity, pose-controllable human videos of unlimited length from a single image. By integrating a dual in-context LoRA finetuning approach with a novel interleaved segment generation strategy using background KV-sharing, PoseGen effectively resolves the critical challenges of identity drift and temporal inconsistency. Our experiments demonstrate that PoseGen establishes a new state-of-the-art, significantly outperforming existing methods in identity preservation, motion control, and long-term coherence, all while requiring a fraction of the typical training data.

## References

- Balaji, Y.; Min, M. R.; Bai, B.; Chellappa, R.; and Graf, H. P. 2019. Conditional GAN with Discriminative Filter Generation for Text-to-Video Synthesis. In *IJCAI*, volume 1, 2.
- Cai, M.; Cun, X.; Li, X.; Liu, W.; Zhang, Z.; Zhang, Y.; Shan, Y.; and Yue, X. 2025. Ditctrl: Exploring attention control in multi-modal diffusion transformer for tuning-free multi-prompt longer video generation. In *Proceedings of the Computer Vision and Pattern Recognition Conference*, 7763–7772.
- Cao, M.; Wang, X.; Qi, Z.; Shan, Y.; Qie, X.; and Zheng, Y. 2023. Masactrl: Tuning-free mutual self-attention control for consistent image synthesis and editing. In *Proceedings of the IEEE/CVF international conference on computer vision*, 22560–22570.
- Cao, Z.; Hidalgo Martinez, G.; Simon, T.; Wei, S.; and Sheikh, Y. A. 2019. OpenPose: Realtime Multi-Person 2D Pose Estimation using Part Affinity Fields. *IEEE Transactions on Pattern Analysis and Machine Intelligence*.
- Caron, M.; Touvron, H.; Misra, I.; Jégou, H.; Mairal, J.; Bojanowski, P.; and Joulin, A. 2021. Emerging properties in self-supervised vision transformers. In *Proceedings of the IEEE/CVF international conference on computer vision*, 9650–9660.
- Chen, K.; Wang, J.; Pang, J.; Cao, Y.; Xiong, Y.; Li, X.; Sun, S.; Feng, W.; Liu, Z.; Xu, J.; et al. 2019. MMDetection: Open mmlab detection toolbox and benchmark. *arXiv* preprint arXiv:1906.07155.
- Chen, Y.; Liang, S.; Zhou, Z.; Huang, Z.; Ma, Y.; Tang, J.; Lin, Q.; Zhou, Y.; and Lu, Q. 2025. HunyuanVideo-Avatar: High-Fidelity Audio-Driven Human Animation for Multiple Characters. arXiv:2505.20156.
- Deng, J.; Guo, J.; Xue, N.; and Zafeiriou, S. 2019. Arcface: Additive angular margin loss for deep face recognition. In *Proceedings of the IEEE/CVF conference on computer vision and pattern recognition*, 4690–4699.
- Gan, Q.; Ren, Y.; Zhang, C.; Ye, Z.; Xie, P.; Yin, X.; Yuan, Z.; Peng, B.; and Zhu, J. 2025. HumanDiT: Pose-Guided Diffusion Transformer for Long-form Human Motion Video Generation. *arXiv preprint arXiv:2502.04847*.
- Guo, Y.; Yang, C.; Rao, A.; Liang, Z.; Wang, Y.; Qiao, Y.; Agrawala, M.; Lin, D.; and Dai, B. 2024. AnimateDiff: Animate Your Personalized Text-to-Image Diffusion Models without Specific Tuning. *International Conference on Learning Representations*.
- Henschel, R.; Khachatryan, L.; Poghosyan, H.; Hayrapetyan, D.; Tadevosyan, V.; Wang, Z.; Navasardyan, S.; and Shi, H. 2025. Streamingt2v: Consistent, dynamic, and extendable long video generation from text. In *Proceedings of the Computer Vision and Pattern Recognition Conference*, 2568–2577.
- Heusel, M.; Ramsauer, H.; Unterthiner, T.; Nessler, B.; and Hochreiter, S. 2017. Gans trained by a two time-scale update rule converge to a local nash equilibrium. *Advances in neural information processing systems*, 30.

- Ho, J.; Jain, A.; and Abbeel, P. 2020. Denoising diffusion probabilistic models. *Advances in neural information processing systems*, 33: 6840–6851.
- Hore, A.; and Ziou, D. 2010. Image quality metrics: PSNR vs. SSIM. In 2010 20th international conference on pattern recognition, 2366–2369. IEEE.
- Hu, E. J.; Shen, Y.; Wallis, P.; Allen-Zhu, Z.; Li, Y.; Wang, S.; Wang, L.; Chen, W.; et al. 2022. Lora: Low-rank adaptation of large language models. *ICLR*, 1(2): 3.
- Hu, L. 2024. Animate anyone: Consistent and controllable image-to-video synthesis for character animation. In *Proceedings of the IEEE/CVF Conference on Computer Vision and Pattern Recognition*, 8153–8163.
- Hu, T.; Yu, Z.; Zhou, Z.; Liang, S.; Zhou, Y.; Lin, Q.; and Lu, Q. 2025. HunyuanCustom: A Multimodal-Driven Architecture for Customized Video Generation. *arXiv* preprint *arXiv*:2505.04512.
- Jafarian, Y.; and Park, H. S. 2021. Learning high fidelity depths of dressed humans by watching social media dance videos. In *Proceedings of the IEEE/CVF Conference on Computer Vision and Pattern Recognition*, 12753–12762.
- Jiang, Z.; Han, Z.; Mao, C.; Zhang, J.; Pan, Y.; and Liu, Y. 2025. Vace: All-in-one video creation and editing. *arXiv* preprint arXiv:2503.07598.
- Jocher, G.; Chaurasia, A.; Stoken, A.; Borovec, J.; Kwon, Y.; Michael, K.; Fang, J.; Yifu, Z.; Wong, C.; Montes, D.; et al. 2022. ultralytics/yolov5: v7.0 yolov5 sota realtime instance segmentation. *Zenodo*.
- Khirodkar, R.; Bagautdinov, T.; Martinez, J.; Zhaoen, S.; James, A.; Selednik, P.; Anderson, S.; and Saito, S. 2024. Sapiens: Foundation for human vision models. In *European Conference on Computer Vision*, 206–228. Springer.
- Kong, W.; et al. 2024. HunyuanVideo: A Systematic Framework For Large Video Generative Models. *arXiv preprint arXiv:2412.03603*.
- Li, H.; Li, Y.; Yang, Y.; Cao, J.; Zhu, Z.; Cheng, X.; and Chen, L. 2024. DisPose: Disentangling Pose Guidance for Controllable Human Image Animation. *arXiv* preprint *arXiv*:2412.09349.
- Lin, G.; Jiang, J.; Yang, J.; Zheng, Z.; and Liang, C. 2025. OmniHuman-1: Rethinking the Scaling-Up of One-Stage Conditioned Human Animation Models. *arXiv preprint arXiv:2502.01061*.
- Luo, Y.; Rong, Z.; Wang, L.; Zhang, L.; Hu, T.; and Zhu, Y. 2025. DreamActor-M1: Holistic, Expressive and Robust Human Image Animation with Hybrid Guidance. *arXiv* preprint arXiv:2504.01724.
- Peebles, W.; and Xie, S. 2022. Scalable Diffusion Models with Transformers. *arXiv preprint arXiv:2212.09748*.
- Peebles, W.; and Xie, S. 2023. Scalable diffusion models with transformers. In *Proceedings of the IEEE/CVF international conference on computer vision*, 4195–4205.
- Qiu, H.; Xia, M.; Zhang, Y.; He, Y.; Wang, X.; Shan, Y.; and Liu, Z. 2023. Freenoise: Tuning-free longer video diffusion via noise rescheduling. *arXiv preprint arXiv:2310.15169*.

- Radford, A.; Kim, J. W.; Hallacy, C.; Ramesh, A.; Goh, G.; Agarwal, S.; Sastry, G.; Askell, A.; Mishkin, P.; Clark, J.; et al. 2021. Learning transferable visual models from natural language supervision. In *International conference on machine learning*, 8748–8763. PmLR.
- Rombach, R.; Blattmann, A.; Lorenz, D.; Esser, P.; and Ommer, B. 2022. High-Resolution Image Synthesis with Latent Diffusion Models. In *Proceedings of the IEEE/CVF Conference on Computer Vision and Pattern Recognition (CVPR)*, 10684–10695.
- Ruiz, N.; Li, Y.; Jampani, V.; Pritch, Y.; Rubinstein, M.; and Aberman, K. 2023. Dreambooth: Fine tuning text-to-image diffusion models for subject-driven generation. In *Proceedings of the IEEE/CVF Conference on Computer Vision and Pattern Recognition*.
- Sohl-Dickstein, J.; Weiss, E.; Maheswaranathan, N.; and Ganguli, S. 2015. Deep unsupervised learning using nonequilibrium thermodynamics. In *International conference on machine learning*, 2256–2265. pmlr.
- Su, J.; Ahmed, M.; Lu, Y.; Pan, S.; Bo, W.; and Liu, Y. 2024. Roformer: Enhanced transformer with rotary position embedding. *Neurocomputing*, 568: 127063.
- Tan, Z.; Liu, S.; Yang, X.; Xue, Q.; and Wang, X. 2024. Ominicontrol: Minimal and universal control for diffusion transformer. *arXiv preprint arXiv:2411.15098*.
- Tu, S.; Xing, Z.; Han, X.; Cheng, Z.-Q.; Dai, Q.; Luo, C.; and Wu, Z. 2025. Stableanimator: High-quality identity-preserving human image animation. In *Proceedings of the Computer Vision and Pattern Recognition Conference*, 21096–21106.
- Unterthiner, T.; Van Steenkiste, S.; Kurach, K.; Marinier, R.; Michalski, M.; and Gelly, S. 2018. Towards accurate generative models of video: A new metric & challenges. *arXiv* preprint arXiv:1812.01717.
- Vaswani, A.; Shazeer, N.; Parmar, N.; Uszkoreit, J.; Jones, L.; Gomez, A. N.; Kaiser, Ł.; and Polosukhin, I. 2017. Attention is all you need. *Advances in neural information processing systems*, 30.
- Wan, T.; Wang, A.; Ai, B.; Wen, B.; Mao, C.; Xie, C.-W.; Chen, D.; Yu, F.; Zhao, H.; Yang, J.; et al. 2025. Wan: Open and advanced large-scale video generative models. *arXiv* preprint arXiv:2503.20314.
- Wang, X.; Zhang, S.; Gao, C.; Wang, J.; Zhou, X.; Zhang, Y.; Yan, L.; and Sang, N. 2024. Unianimate: Taming unified video diffusion models for consistent human image animation. *arXiv* preprint arXiv:2406.01188.
- Wang, X.; Zhang, S.; Tang, L.; Zhang, Y.; Gao, C.; Wang, Y.; and Sang, N. 2025. Unianimate-dit: Human image animation with large-scale video diffusion transformer. *arXiv* preprint arXiv:2504.11289.
- Wang, Z.; Bovik, A. C.; Sheikh, H. R.; and Simoncelli, E. P. 2004. Image quality assessment: from error visibility to structural similarity. *IEEE transactions on image processing*, 13(4): 600–612.
- Wu, H.; Zhang, Z.; Zhang, W.; Chen, C.; Liao, L.; Li, C.; Gao, Y.; Wang, A.; Zhang, E.; Sun, W.; et al. 2023. Q-align:

- Teaching lmms for visual scoring via discrete text-defined levels. *arXiv preprint arXiv:2312.17090*.
- Yang, A.; Yang, B.; Hui, B.; Zheng, B.; Yu, B.; Zhou, C.; Li, C.; Liu, D.; Huang, F.; et al. 2024a. Qwen2 technical report. *arXiv preprint arXiv:2407.10671*.
- Yang, Z.; Teng, J.; Zheng, W.; Ding, M.; Huang, S.; Xu, J.; Yang, Y.; Hong, W.; Zhang, X.; Feng, G.; et al. 2024b. Cogvideox: Text-to-video diffusion models with an expert transformer. *arXiv* preprint *arXiv*:2408.06072.
- Zhang, L.; Rao, A.; and Agrawala, M. 2023. Adding conditional control to text-to-image diffusion models. In *Proceedings of the IEEE/CVF international conference on computer vision*, 3836–3847.
- Zhang, R.; Isola, P.; Efros, A. A.; Shechtman, E.; and Wang, O. 2018. The unreasonable effectiveness of deep features as a perceptual metric. In *Proceedings of the IEEE conference on computer vision and pattern recognition*, 586–595.
- Zhang, Y.; Gu, J.; Wang, L.-W.; Wang, H.; Cheng, J.; Zhu, Y.; and Zou, F. 2025. MimicMotion: High-Quality Human Motion Video Generation with Confidence-aware Pose Guidance. In *International Conference on Machine Learning*.
- Zhou, J.; Wang, B.; Chen, W.; Bai, J.; Li, D.; Zhang, A.; Xu, H.; Yang, M.; and Wang, F. 2024. RealisDance: Equip controllable character animation with realistic hands. *arXiv* preprint arXiv:2409.06202.

# **Supplementary Material**

In this supplementary material, we present more details on our training data, implementation, additional qualitative results, ablation studies, and limitations.

# S1 Training Data

## S1.1 Data Construction

We collect human-centric videos that capture the movement of a single person, such as dancing or live broadcasting, from various online platforms. To ensure the quality of these videos for training, we employ a comprehensive filtering process. Initially, the collected videos undergo a manual screening to discard samples containing undesirable elements such as abrupt scene changes, background jitter, or superimposed special effects. Following this, we apply an automated filtering pipeline to only preserve samples that simultaneously meet the following criteria. (1) Visual Quality. We adopt the image and video quality scorers provided by Q-Align (Wu et al. 2023) to assess the visual quality of a collected video. A threshold of 0.7 is applied for both scorers to exclude low-quality samples. (2) Human Presence. We uniformly sample a set of frames from a video and extract human bounding boxes using RTMDet (Chen et al. 2019). We then compute the human area ratio according to the estimated bounding boxes. Videos with an average ratio below 0.3 are discarded to eliminate those with insufficient human presence. Meanwhile, this moderate threshold effectively retains videos where humans are captured in close-up, medium, or full shots. (3) Facial Confidence. We apply YOLO (Jocher et al. 2022) to extract bounding box annotations for the categories "face" and "head" in each sampled frame. Videos with an average confidence score exceeding 0.75 are retained to ensure clear visibility of human face and head regions. This filtering choice helps avoid significant occlusions from masks, hats, or similar accessories, which can detrimentally affect the performance of identity-preserving human video generation. Finally, we obtain a training dataset that comprises 7,005 high-quality video clips for LoRA finetuning.

#### S1.2 Data Preprocessing

We leverage Sapiens (Khirodkar et al. 2024), a family of human vision models, to predict pose skeleton maps and hand normal maps for training videos. Regarding pose estimation, the score threshold and the Intersection-over-Union (IoU) threshold for human bounding box detection are both set to 0.3. We render OpenPose (Cao et al. 2019)-style body and hand keypoints while discarding facial keypoints, in order to avoid identity leakage from the driving video to the generated subject. To balance precision and recall, we empirically set the confidence threshold to 0.3 for body keypoints and 0.7 for hand keypoints to ensure accurate pose skeletons. For hand normal prediction, we first apply the surface normal prediction model of Sapiens to generate normal maps for the entire frame, and then use its body-part segmentation model

to localize the desired hand regions. Considering that the quality of hand regions in a training video is often affected by motion blurs, a dropout rate of 0.1 is applied to both hand skeletons and surface normals in order to decouple the strong reliance on these conditions and promote model robustness. We adopt Qwen2.5-7B-Instruct (Yang et al. 2024a) as our text encoder to generate text prompts for reference images. The structure of a prompt typically begins with the image style, followed by a detailed description of the subject and the background, and ends with the type of the camera shot, which is similar to the prompt distribution of Wan2.1 post-training captions.

# S2 Additional Implementation Details

Our model is built upon the checkpoint of Wan2.1 Imageto-Video (I2V) 14B model (Wan et al. 2025). The learnable parameters in the reference image patchifier are initialized by copying those in the noisy video patchifier. To prevent color-related artifacts that we observed in early experiments when concatenating hand normal maps with pose skeletons, we devised an alternative integration strategy. Instead of a simple concatenation, we process the hand normal maps through a separate patchifier and then add its output to the pose skeleton features. This convolution-addition scheme effectively fuses geometric information without introducing color spillover. We then append a zero-initialized linear projection layer after the 3D convolutional layer in the separated hand patchifier to suppress its influence at the beginning of the training process, inspired by the design of ControlNet (Zhang, Rao, and Agrawala 2023). During training, the learning rate is linearly warmed up to 1e-4 over the first 10% of the total training steps, followed by a cosine annealing scheduler for the remaining steps. The LoRA rank and alpha are both set to 16.

#### S3 Additional Qualitative Results

We present more qualitative results of pose-driven human video generation in Fig. S1. These visualizations showcase that our model effectively synthesizes realistic human videos while preserving identity consistency across diverse scenes and complex motion patterns. Notably, PoseGen exhibits impressive generalization capabilities beyond the real-human videos it was trained on. As demonstrated in the bottom row of Fig. S1, by first applying a pose retargeting process (Wang et al. 2025) to the driving motion, our model can successfully animate out-of-domain subjects like cartoon characters, faithfully transferring the motion while preserving the distinct artistic style.

### **S4** Additional Ablation Study

Following the settings in DiTCtrl (Cai et al. 2025), we perform background KV-sharing at early denoising timesteps and at deep transformer layers. To further evaluate the effect of denoising timesteps and transformer layers, we conducted



Figure S1: Additional qualitative results of pose-controllable human video generation. The reference images are displayed at the first column.

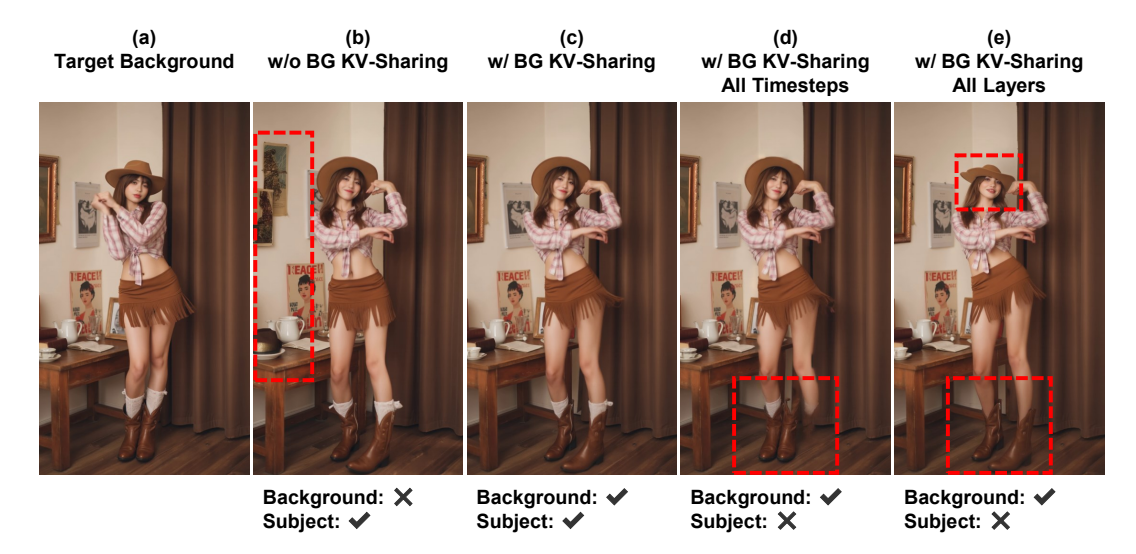


Figure S2: Ablation study on background KV-sharing in terms of denoising timesteps and transformer layers. (a) The source segment with the target background. (b) Background KV-sharing is not applied. (c) Background KV-sharing is applied to the first five timesteps and the last ten layers. (d) Background KV-sharing is applied to all timesteps and the last ten layers. (e) Background KV-sharing is applied to the first five timesteps and all layers.

an ablation on the background KV-sharing mechanism, and the results are presented in Fig. S2. As shown in Fig. S2, background KV-sharing not only preserves the desired background from the source segment when generating the current segment, but also successfully drives the subject according to the pose signals without introducing noticeable artifacts. Specifically, applying background KV-sharing across all denoising timesteps causes inadvertent propagation of human pose information from the source to the current segment, resulting in overlapping poses and reduced motion fidelity. In contrast, implementing background KV-sharing across all transformer layers allows low-level visual features to leak from the source segment, leading to visual artifacts on the subject. These observations corroborate the findings in MasaCtrl (Cao et al. 2023), which indicate that source background is primarily conveyed during initial denoising steps and in deeper network layers. Our approach retains the first denoising step, a minor deviation from DiTCtrl (Cai et al. 2025) and MasaCtrl (Cao et al. 2023), to ensure consistency for the identical background expected across video segments.

#### S5 Limitations

Despite its strong performance, PoseGen also exhibits a few limitations. First, the interleaved segment-wise generation approach may introduce subtle drift in fine-grained details (such as the subject's delicate accessories) or in occluded regions of the reference image. Second, the model's ability to create seamless long videos hinges on the selected source segment having a static background, as any source variations can lead to unnatural artifacts in the segments to be generated. Third, in terms of controllability, our framework does not support nuanced control of facial expressions, which we leave for future work.